IMPACT OF RAY EFFECTS ON A^{3}MCNP PERFORMANCE FOR A PURELY ABSORBING MEDIUM WITH VOID REGION

Apisit Patchimpattapong and Alireza Haghighat
Penn State University
Nuclear Engineering Program
University Park, PA 16802
axp227@psu.edu; haghighat@psu.edu

ABSTRACT

This paper analyzes the performance of A^{3}MCNP™ (Automated Adjoint Accelerated MCNP) for a purely absorbing medium with void region. A^{3}MCNP™ is based on the CADIS (Consistent Adjoint Driven Importance Sampling) methodology, which uses a deterministic 3-D importance function, to determine variance reduction parameters. A^{3}MCNP™ automatically prepares necessary input files for adjoint transport calculation using the TORT discrete ordinates (S_N) code. In a purely absorbing medium with void region, the S_N method suffers from the ray effects. The impact of the ray effects on the performance of A^{3}MCNP™ is investigated using different uniform mesh distributions. It is demonstrated that for an adjoint function distribution with no oscillation (ray effects), A^{3}MCNP™ can yield significant speedups over an analog Monte Carlo calculation, for a medium containing pure absorber and void regions.

1. INTRODUCTION

For solving shielding problems, one of the most widely used approaches is the Monte Carlo method. It offers several advantages including accurate representation of problem geometry and physics. However its disadvantages include a significant amount of computation time for achieving statistically reliable results. For deep-penetration shielding calculations, analog Monte Carlo methods are not practical due to ineffectiveness of handling poorly scattering media. Consequently, non-analog Monte Carlo methods are used instead. There are several effective variance reduction techniques such as the weight-window splitting/roulette, exponential transformation, and source biasing. Nevertheless, their use for large or complex problems is not straightforward because of the need for space, energy, and in certain situations angular dependent parameters.

The particle “Importance” function, commonly referred to as adjoint function, has long been recognized for its benefit of providing detailed physical information inside the system. Hence, it is practical to establish the variance reduction parameters based on the importance function. There are a number of methodologies being developed for estimation of the particle “importance” and its utilization for variance reduction [*1-4*]. Among these, the CADIS (Consistent Adjoint Driven Importance Sampling) methodology [*5,6*] was developed at the Penn State University. This methodology utilizes a 3-D S_N importance function distribution for source and transport biasing consistently within the weight-window technique. Further, A^{3}MCNP™ (Automated Adjoint Accelerated MCNP) [*5,6,8*], a new version of MCNP [*7*], has been developed, based on the CADIS methodology. A^{3}MCNP™ automatically prepares input files (including mesh, source, and material cross sections) for an S_N transport code for determination of the importance function. The current version of A^{3}MCNP™ uses the TORT S_N code [*9*].

A^{3}MCNP™ has been used for a PWR cavity dosimetry calculation [*6*], for determination of the DPA (Displacement Per Atom) at a BWR core shroud [*10*], and for simulation of a shipping cask [*5*]. In this paper, we utilize A^{3}MCNP™ to calculate flux at various sets of locations in a medium containing pure absorber and void region. For such a medium, the discrete ordinates method suffers from the ray effects [*11*], which may yield a flux (or importance function) distribution with unphysical oscillations. This results in a fluctuation of variance reduction parameters in an adjacent region for transport biasing, which lowers the performance of A^{3}MCNP™. Since A^{3}MCNP™ relies on the use of S_N adjoint function, it is necessary to investigate the impact of the “ray effects”. To address this issue, we have examined the effect of different combinations of spatial and angular discretization on the performance of A^{3}MCNP™.

The next section discusses the theory of the CADIS methodology. The section after that describes A^{3}MCNP™. Then, the approach considered for this study is described, followed by results and discussions. The last section summarizes and concludes the paper.

2. THEORY – CADIS METHODOLOGY

The CADIS (Consistent Adjoint Driven Importance Sampling) methodology utilizes the space-energy weight-window technique to perform a consistent source and transport biasing. From the importance sampling method [*12*], the biased source [*5,6*] can be written as

$$\hat{q}(r,E)=\frac{\phi^{+}(r,E)q(r,E)}{\int\int_{V}\int_{E}\phi^{+}(r,E)q(r,E)drdE}=\frac{\phi^{+}(r,E)q(r,E)}{R} \qquad (1)$$

with an associated statistical weight of

$$W(r,E) = \frac{\int\int_{V\,E} \phi^{+}(r,E)q(r,E)drdE}{\phi^{+}(r,E)} = \frac{R}{\phi^{+}(r,E)} \qquad (2)$$

where R, $\phi^{+}(r,E)$, $q(r,E)$, and $\hat{q}(r,E)$ are the detector response, the importance function, unbiased source and biased source, respectively.

Equation 1 indicates that source particles are sampled, based on the ratio of their contribution to the detector response. Therefore, their weight must be adjusted accordingly.

For transport biasing, the transformed equation based on the integral transport equation [*5,6,11*] can be written as

$$\hat{\phi}(r,E) = \int_{V}\int_{E} \hat{K}(r',E' \to r,E)\hat{\phi}(r',E')dr'dE' + \hat{q}(r,E) \qquad (3)$$

and

$$\hat{K}(r',E' \to r,E) = K(r',E' \to r,E)\left[\frac{\phi^{+}(r,E)}{\phi^{+}(r',E')}\right] \qquad (4)$$

where $K(r',E' \to r,E)$, $\hat{K}(r',E' \to r,E)$, $\phi^{+}(r,E)$, and $\phi^{+}(r',E')$ are the transport kernel (probability of transfer from phase space (r',E') to (r,E)), the biased kernel, and the importance function at phase space (r',E') and (r',E'), respectively.

Since the transport kernel $K(r',E' \to r,E)$ is not known, the particle transport between any events is simulated in the normal "unbiased" approach. The number of particles emerging in phase space (r,E) from an event in phase space (r',E') is then altered by the ratio of importances, $\phi^{+}(r,E)/\phi^{+}(r',E')$. If particles are moving toward more importance region (the ratio > 1), particles are created (splitting). Conversely, particles are terminated (roulette) if they are moving toward lower importance region (the ratio < 1). The statistical weight of the particles must be consequently modified as

$$W(r,E) = W(r',E')\left[\frac{\phi^{+}(r',E')}{\phi^{+}(r,E)}\right] \qquad (5)$$

Equation (3) demonstrates the "consistent" use of the importance sampling method and the transport biasing.

3. DEVELOPMENT OF A^{3}MCNP AND ITS USE

To utilize the CADIS methodology, one has to develop a mesh distribution and a multi-group cross section files for performing a three-dimensional discrete ordinates (S_N) adjoint calculation. This procedure, however, is not straightforward and requires a significant amount of time and knowledge. To remove this difficulty, a new version of the MCNP code, A^{3}MCNP™ (Automated Adjoint Accelerated MCNP) has been developed. A^{3}MCNP™ performs the following tasks.

i. Generation of a mesh distribution for the deterministic S_N calculation. (Mesh generator utility first generates a uniform mesh distribution to extract information on material distribution, and then a back-thinning process prepares a variable mesh distribution.)
ii. Preparation of an input file for the TORT S_N code.
iii. Determination of material compositions and preparation of the necessary input files for the GIP code [*9*] for generation of multi-group cross sections.
iv. Reading the "importance" function and preparing a biased source based on Equation 1.
v. Superimposing the deterministic S_N spatial-mesh distribution and energy-group structure onto the Monte Carlo Model in a "transparent" manner.
vi. Calculating space- and energy-dependent weight-window lower bounds (w_l) for the "transparent" space-energy mesh according to

$$w_l(r,E) = \frac{R}{\phi^+(r,E)} \cdot \frac{1}{\left(\frac{C_u+1}{2}\right)}$$

where ϕ^+ is the scalar adjoint function, $C_u = w_u / w_l$ is the ratio of upper and lower weight window values.
vii. Updating the particle weight, as each particle is transported through the "transparent" mesh.

4. METHODOLOGY

We model a "square void" problem, which is one of three benchmark problems proposed by Kobayashi at OECD/NEA in 1996 [*13*]. A schematic of this problem is shown in Figures 1. It consists of three material regions: source, void and absorber. The source strength is 1.0 n/cm^3/s. One-group cross sections are 10^{-4} cm^{-1} for the void, and 0.1 cm^{-1} for the source and the absorber. The reflective boundary conditions are prescribed at the inside boundaries (left, back and bottom), whereas the vacuum boundary conditions are prescribed at the outside boundaries (right, front and top).

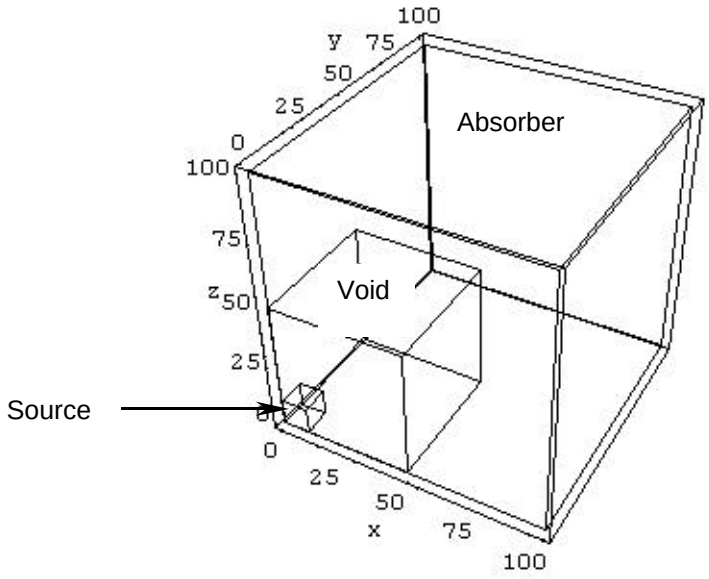

Figure 1 – A schematic of a "Square Void" Problem.

We determine the accuracy of A^{3}MCNP™ calculation by comparing cell-averaged flux values from A^{3}MCNP™ with analytical solutions [*14*] at various sets of locations. Fluxes are tallied at the center of 10x10x10 cm^3 meshes in 1x1x1 cm^3 tally volumes. The tally locations are as follows,

Case 1A) Along the y-axis at 5 cm intervals (at x = 5, z = 5 cm)
Case 1B) Along the major diagonal at center of each cell (starting at x = 5, y = 5, z = 5 cm)
Case 1C) Parallel to the x-axis at 5 cm intervals (at y = 55, z = 5 cm)

Then, we examine the performance of A^{3}MCNP™ by comparing its FOM's (Figure-of-Merits) with those from MCNP. FOM is defined by

$$\mathrm{FOM} = \frac{1}{\mathrm{R}^2 \mathrm{T}}$$

where R is the relative error $\left(\mathrm{R} = \frac{\sigma_{\mathrm{X}} / \sqrt{\mathrm{N}}}{\overline{\mathrm{X}}} \right)$ and T is CPU minutes.

As discussed earlier, A^{3}MCNP™ utilizes the 3-D S_N adjoint function to generate the variance reduction parameters. Since the medium of interest is made of void and pure absorber, source particles can be terminated via two mechanisms: absorption or crossing surface boundaries. For any sets of locations of observation aligned on the same direction from the source, one adjoint source at the last location is sufficient to provide appropriate weight-window parameters. Otherwise, the adjoint source must be placed at every point of observation independently.

Since we use the deterministic TORT S_N code to calculate the 3-D adjoint function, we have to deal with the fact that in a purely absorbing medium with void region, the discrete ordinates method suffers from the ray effects. In the next section, we will examine different spatial mesh distributions in order to achieve minimal ray effects.

All MCNP and A^{3}MCNP calculations are performed on a 332 MHz PowerPC processor at the Penn State University.

5. RESULTS AND DISCUSSIONS

Adjoint function distribution

In this section, we test different spatial mesh distributions for the deterministic S_N calculation in order to minimize the ray effects. For this test, we use Case 1A, along the y-axis at 5 cm intervals (at x = 5, z = 5 cm). We reduce the size of the model to a 10x100x10 cm^3 duct. A schematic of the simplified model is shown in Figure 2. Due to a purely absorbing medium with void region, particles will not come back after crossing surface boundaries and, hence, they no longer contribute to the detector response. Consequently, this simplified model is adequate for Case 1A. Since all three cases contain the same material composition and have similar configurations, the results from this test can be practically applied to them.

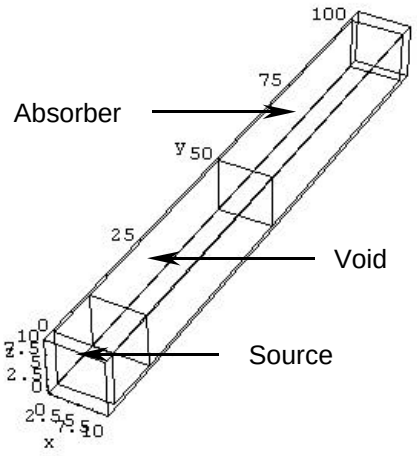

Figure 2 – A Schematic of the Simplified Model of Case 1A.

As discussed in Section 3, A^{3}MCNP™ automatically generates a uniform spatial mesh distribution with an optional back-thinning process for a variable mesh distribution. We have examined numerous spatial mesh distributions, and for brevity, we discuss only three uniform mesh distributions. Since this is a highly directional dependent problem, we use the highest possible level-symmetric quadrature set of S_{20}. We have described in Section 4 that fluxes are tallied at the center of 10x10x10 cm^3 meshes in 1x1x1 cm^3 tally volumes. To determine an effective adjoint (importance) function distribution, the adjoint source is placed at the tally location (detector). This means that the adjoint source assumes the same size and shape as the tally region. However, with a uniform mesh distribution, the size of the adjoint source

depends upon the spatial mesh interval. Table 1 gives the relation between the uniform spatial mesh size and the size of the adjoint source for selected mesh intervals. Figure 3 shows the associated adjoint function distributions.

Table 1 – Relationship Between the Uniform Spatial Mesh Size and the Size of the Adjoint Source.

Spatial Mesh Size (cm)	Number of Meshes Required	Size of Adjoint Source (cm)
5.0	8	10.0
2.5	8	5.0
2.0	1	2.0

Fig. 3 shows that because of the different sizes of the adjoint source, we obtain adjoint function distributions of different magnitudes. For 2.5-cm and 5.0-cm meshes, the adjoint function distributions are virtually smooth but for a 2.0-cm mesh, we observe the ray effects throughout the whole distribution. It suggests that to avoid the ray effects, one shall implement the mesh, at least, larger than 2.0 cm.

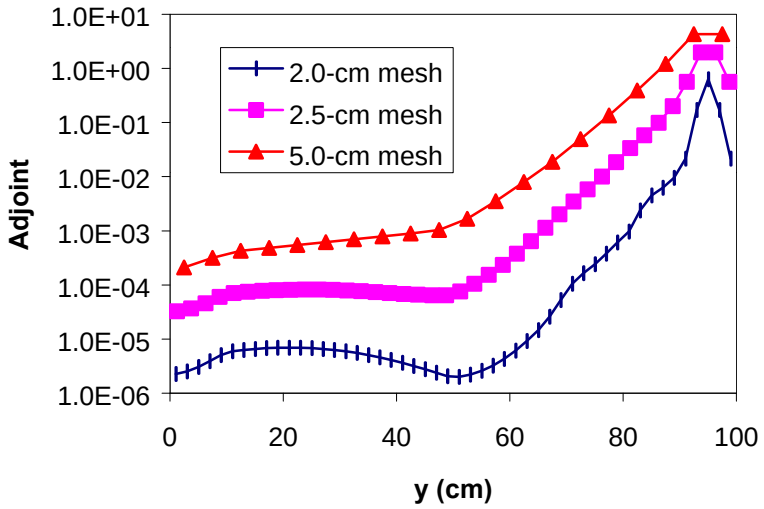

Figure 3 – Adjoint Function Distributions of Different Uniform Mesh Distributions.

Note that for all three cases, we use the same geometric model for both MCNP and A^{3}MCNP™ calculations. To reduce the size of the full model (Figure 1), the simplified one (Figure 2), we set the importance of other regions outside the simplified model to zero.

Table 2 compares fluxes, relative errors, FOM's (Figure-of-Merits) of Case 1A after 60 CPU minutes. In all four calculations, FOM's decrease with distance, as expected, due to the loss of particles in a void or purely absorbing media. The 2.0-cm mesh case has the lowest FOM's, because of the ray effects. The highest FOM's are observed in the 2.5-cm mesh case, because of the following reasons:

1) The 2.5-cm mesh case has a smooth adjoint function distribution;
2) As compared to the 5.0-cm mesh case, the size of the adjoint source of the 2.5-cm mesh case is closer to the size of the "real" adjoint source;
3) In the forward source region (between y = 0 cm and y = 10 cm), compared to the 5.0-cm mesh case, the 2.5-cm mesh case has a more detailed adjoint function distribution. Therefore, A^{3}MCNP™ does a more effective transport biasing (i.e., splits the important particles, while roulettes the unimportant ones) within the source region.

It is worth noting that even the 5.0-cm mesh case yields a decent improvement in the FOM, as high as a factor of 5 over MCNP.

Based on the results of this analysis, all the solutions in the remainder of this paper are based on a 2.5-cm uniform mesh adjoint model.

Case 1A – Along the y-axis at 5 cm intervals (at x = 5, z = 5 cm)

A^{3}MCNP does transport biasing within the source and the pure absorber. In the absorber region, the biasing becomes more effective because of the larger size. Furthermore, the model of Case 1A is simplified such that the particles that do not travel in the directions toward the tally location will be quickly terminated when crossing the surface boundaries. Therefore, A^{3}MCNP™ yields higher FOM's than those of the unbiased case, especially in the absorber region.

Table 2 – Calculated Fluxes and Associated Statistics of Case 1A After 60 CPU Minutes.

x	y (cm)	z	Analytical Method	MCNP			A^{3}MCNP 2.0-cm mesh		
				Flux	Error (%)	FOM	Flux	Error (%)	FOM
5	5	5	5.9566E+00	5.9564E+00	0.280	2125.85	5.9574E+00	0.700	340.14
5	15	5	1.3719E+00	1.3661E+00	0.600	462.96	1.3732E+00	1.590	65.93
5	25	5	5.0087E-01	5.0582E-01	1.000	166.67	5.0467E-01	2.710	22.69
5	35	5	2.5243E-01	2.5094E-01	1.420	82.66	2.6309E-01	3.790	11.60
5	45	5	1.5026E-01	1.4872E-01	1.860	48.18	1.5312E-01	4.780	7.29
5	55	5	5.9529E-02	6.0432E-02	2.910	19.68	5.6049E-02	6.710	3.70
5	65	5	1.5328E-02	1.5330E-02	5.800	4.95	1.6361E-02	12.570	1.05
5	75	5	4.1769E-03	4.3489E-03	10.970	1.38	3.7636E-03	10.500	1.51
5	85	5	1.1853E-03	1.4250E-03	19.080	0.46	1.0667E-03	16.170	0.64
5	95	5	3.4685E-04	2.7823E-04	40.540	0.10	3.1448E-04	18.400	0.49
x	y (cm)	z	Analytical Method	A^{3}MCNP 2.5-cm mesh			A^{3}MCNP 5.0-cm mesh		
				Flux	Error (%)	FOM	Flux	Error (%)	FOM
5	5	5	5.9566E+00	5.9391E+00	0.220	3443.53	5.9758E+00	0.290	1981.77
5	15	5	1.3719E+00	1.3773E+00	0.490	694.16	1.3644E+00	0.580	495.44
5	25	5	5.0087E-01	4.9651E-01	0.830	241.93	4.9548E-01	0.980	173.54
5	35	5	2.5243E-01	2.5716E-01	1.190	117.69	2.5106E-01	1.390	86.26
5	45	5	1.5026E-01	1.4924E-01	1.520	72.14	1.5098E-01	1.790	52.02
5	55	5	5.9529E-02	5.9919E-02	2.400	28.94	6.0286E-02	2.790	21.41
5	65	5	1.5328E-02	1.4800E-02	4.070	10.06	1.6602E-02	4.620	7.81
5	75	5	4.1769E-03	4.0662E-03	5.220	6.12	4.6713E-03	6.130	4.44
5	85	5	1.1853E-03	1.0547E-03	6.950	3.45	1.5513E-03	8.730	2.19
5	95	5	3.4685E-04	3.3235E-04	8.280	2.43	4.1118E-04	17.780	0.53

Case 1B – Along the major diagonal at center of each cell (starting at x = 5, y = 5, z = 5 cm)

Table 3 compares fluxes, relative errors, FOM's (Figure-of-Merits) of Case 1B after 1000 CPU minutes for MCNP and 300 CPU minutes for A^{3}MCNP™. Since the size of the source is small and the tally locations (locations of observation) are along the major diagonal, the solid angle through which the tally location can see the source is very small. Due to a purely absorbing medium with void region, only particles that travel through this solid angle can reach to the location of observation. The "importance" function of particles outside the solid angle must be zero. The discrete ordinates method has a limited number of directions; hence, there are not enough directions to accurately represent the importance distribution within and beyond the solid angle. This is especially important for this location, because only a small segment of the source can contribute to the problem objectives; therefore, the transport biasing becomes ineffective and costly. In the absorber region, however, the particles have to travel more than 8 MFPs to reach the tally location. Therefore, the transport biasing becomes more effective and necessary as the particles penetrate farther within the absorber. For example at x = 95, y = 95, z = 95 cm, we obtain a FOM that is larger by a factor of 40 compared to than the unbiased case.

Table 3 - Calculated Fluxes and Associated Statistics of Case 1B After 1000 CPU Minutes for MCNP and 300 CPU Minutes for A^{3}MCNP.

x	y	z	Analytical Method	MCNP			A^{3}MCNP		
(cm)							2.5-cm mesh		
				Flux	Error (%)	FOM	Flux	Error (%)	FOM
5	5	5	5.9566E+00	5.9475E+00	0.040	6250.00	5.9531E+00	0.090	4115.23
15	15	15	4.7075E-01	4.7016E-01	0.150	444.44	4.7044E-01	0.320	325.52
25	25	25	1.6997E-01	1.6971E-01	0.260	147.93	1.7048E-01	0.530	118.67
35	35	35	8.6833E-02	8.6804E-02	0.360	77.16	8.7293E-02	0.750	59.26
45	45	45	5.2513E-02	5.2288E-02	0.460	47.26	5.2350E-02	0.960	36.17
55	55	55	1.3338E-02	1.3447E-02	0.900	12.35	1.3515E-02	1.890	9.33
65	65	65	1.4587E-03	1.4560E-03	2.700	1.37	1.5158E-03	4.230	1.86
75	75	75	1.7536E-04	1.6970E-04	8.060	0.15	2.0221E-04	7.910	0.53
85	85	85	2.2461E-05	2.7073E-05	19.640	0.03	2.1149E-05	10.030	0.33
95	95	95	3.0103E-06	2.9870E-06	60.960	0.003	2.9327E-06	17.460	0.11

Case 1C – Parallel to the x-axis at 5 cm intervals (at y = 55, z = 5 cm)

As discussed in Section 4, for any sets of locations of observation that are not on the same direction from the source, the adjoint source must be placed at every location independently. Therefore, we setup ten separate models for both MCNP and A^{3}MCNP™, based on the locations of observation (tally locations). For instance, Figures 4a and 4b shows schematics of the models of Case 1C for the first two tally locations (x = 5, y = 55, z = 5 cm and x = 15, y = 55, z = 5 cm). To change the size of the model, we set the importance of other regions outside the model to zero.

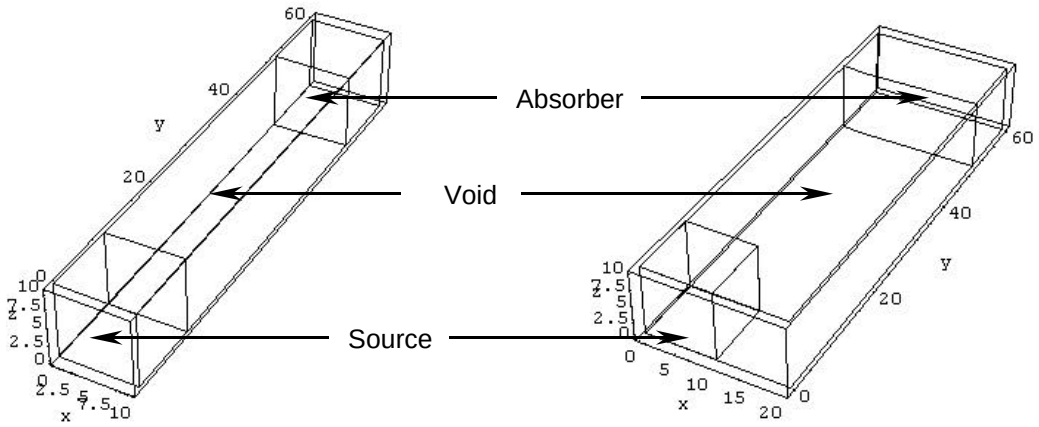

(a) For the first tally location (x = 5, y = 55, z = 5 cm)

(b) For the second tally location (x = 15, y = 55, z = 5 cm)

Figure 4 – Examples of the Models of Case 1C.

Table 4 compares fluxes, relative errors, FOM's (Figure-of-Merits) of Case 1C after 60 CPU minutes. We observe that the behavior of FOM highly depends on the size of the solid angle through which the tally location can "see" the source. For instance, for the second tally location (Figure 4b), the segment of the source region "seen" is significantly smaller than that of the first location. Hence, the A^{3}MCNP™ transport biasing that is performed for both "important" and "unimportant" source particles diminishes the performance (i.e., FOM). However, similar to Cases 1A and 1B, the transport biasing becomes effective and necessary in the absorber region and consequently, A^{3}MCNP™ yields higher FOM's than MCNP.

Table 4 - Calculated Fluxes and Associated Statistics of Case 1C After 60 CPU Minutes.

x	y	z	Analytical Method	MCNP			A^{3}MCNP 2.5-cm mesh		
(cm)				Flux	Error (%)	FOM	Flux	Error (%)	FOM
5	55	5	5.9529E-02	6.0349E-02	2.360	29.92	5.9240E-02	2.040	40.05
15	55	5	5.5025E-02	5.4304E-02	1.190	117.69	5.2967E-02	1.720	56.34
25	55	5	4.8075E-02	4.7873E-02	1.290	100.15	4.9022E-02	2.230	33.51
35	55	5	3.9677E-02	3.9794E-02	3.130	17.01	4.0313E-02	1.870	47.66
45	55	5	3.1637E-02	3.1779E-02	2.710	22.69	3.0834E-02	2.780	21.57
55	55	5	2.3530E-02	2.3634E-02	3.030	18.15	2.3342E-02	2.570	25.23
65	55	5	5.8372E-03	5.9178E-03	3.830	11.36	6.0616E-03	3.750	11.85
75	55	5	1.5673E-03	1.4288E-03	7.700	2.81	1.6065E-03	5.110	6.38
85	55	5	4.5311E-04	1.4151E-04	53.810	0.06	4.4182E-04	8.130	2.52
95	55	5	1.3708E-04	1.0967E-04	45.590	0.08	1.3345E-04	8.720	2.19

Table 5 compares maximum relative errors, FOM's (Figure-of-Merits) and speedups for all cases. We achieve significant speedups in all three cases. In Case 1B, A^{3}MCNP™ yields the largest speedup of ~40, because the point of observation is the farthest (> 8 MFPs) from the source. Note that the computation time of the S_N adjoint function is not included since it is very small (< 1 minute).

Table 5 - Comparison of A^{3}MCNP and MCNP Performances.

Case	Code	Max. Relative Error (%)	FOM	MCNP Speedup (FOM_{A3MCNP}/FOM_{MCNP})
1A[1]	MCNP	40.540	0.101	1.0
	A^{3}MCNP	8.280	2.431	24.0
1B[2]	MCNP	60.960	0.003	1.0
	A^{3}MCNP	17.460	0.109	40.6
1C[1]	MCNP	53.810	0.058	1.0
	A^{3}MCNP	8.720	2.192	38.1

[1] after 60 CPU minutes.
[2] after 1000 CPU minutes for MCNP and 300 CPU minutes for A^{3}MCNP™.

6. SUMMARY AND CONCLUSIONS

This paper examines the performance of A^{3}MCNP™ (Automated Adjoint Accelerated MCNP) for a purely absorbing medium with void region. It also describes the capabilities of the A^{3}MCNP™ code, its automated variance reduction methodology, and the CADIS (Consistent Adjoint Driven Importance Sampling) methodology. The CADIS methodology utilizes the deterministic 3-D S_N importance function for preparation of variance reduction parameters for source and transport biasing consistently within the weight-window technique. Therefore, A^{3}MCNP™ performance is sensitive to its shape. In an absorbing medium, the discrete ordinates method may suffer from the ray effects, resulting in the oscillation of variance reduction parameters and, hence, lowering the A^{3}MCNP™ performance. Different uniform mesh distributions are examined to investigate this issue. With a reasonable uniform mesh distribution of 2.5 cm, A^{3}MCNP™ yields significant speedups (up to 40) over MCNP. It is also worth noting that A^{3}MCNP™ considerably reduces engineering's time and increase reliability of results.

ACKNOWLEDGEMENTS AND TRADEMARKS

A^{3}MCNP™ is a trademark of H & S Advanced Computing Technologies, Inc. (H&SACT), http://www.hsact.com.

The authors would like to express their appreciation to Dr. John C. Wagner, Oak Ridge National Laboratory, for his constructive comments and suggestions.

REFERENCES

[1] Kalos, M. H. “Importance Sampling in Monte Carlo Shielding Calculations: I. Neutron Penetration Through Thick Hydrogen Slabs,” *Nuclear Science and Engineering*, Vol. 16, 1963. p. 227.

[2] Tang, T.S., Stevens, P. N., and Hoffman, T. J., *Methods of Monte Carlo Biasing Using Two-Dimensional Discrete Ordinates Adjoint Flux*, ORNL/TM-5414, Oak Ridge National Laboratory, Oak Ridge, TN, 1976.

[3] Miller, P. C., Wright, G. A., Boyle, G. B., and Power, S. W., "The Use of an Inbuilt Importance Generator for Acceleration of the Monte Carlo Code MCBEND," *Proceedings of the International Conference Physics of Reactor Operation, Design and Computation*, Marseilles, France, April 23-26, 1990, p. 124.

[4] Van Riper et al., K. A., "AVATAR – Automatic Variance Reduction in Monte Carlo Calculations," *Proc. Joint International Conference Mathematical Methods and Supercomputing for Nuclear Applications*, Saratoga Springs. New York, October 6-10, 1997, Vol. 1, American Nuclear Society, 1997, pp. 661-670.

[5] Wagner, J. C., "Acceleration of Monte Carlo Shielding Calculations with an Automated Variance Reduction Technique and Parallel Processing," *Ph.D. Dissertation*, The Pennsylvania State University, 1997.

[6] Wagner, J. C. and Haghighat, A., "Automated Variance Reduction of Monte Carlo Shielding Calculations Using the Discrete Ordinates Adjoint Function," *Nuclear Science and Engineering*, Vol. 128, 1998, pp. 186-208.

[7] Briesmeister, J. F. (Ed.), "*MCNP - A General Monte Carlo Code for N-Particle Transport Code, Version 4A*," LA-12625, Los Alamos National Laboratory, Los Alamos, NM, 1993.

[8] Wagner, J. C. and Haghighat, A., *A^3MCNP™, Automated Adjoint Accelerated MCNP – Users Guide, Rev. 1.0A*, The Pennsylvania State University, April, 1998.

[9] W.A. Rhoades and M.B. Emmett, *DOS: The Discrete Ordinates System*, ORNL/TM-8362, ORNL, Oak Ridge, TN, 1982.

[10] Haghighat, A., Hiruta, H., Petrovic, B., and Wagner, J. C., "Performance of the Automated Adjoint Accelerated MCNP (A^3MCNP) for Simulation of a BWR Core Shroud Problem", *Proceeding of the Mathematics and Computation, Reactor Physics and Environmental Analysis in Nuclear Applications*, Madrid, Spain, September 27-30, 1999, Vol. 2, p. 1381-1391.

[11] Lewis, E. E. and Miller, W. F. Jr., *Computational Methods of Neutron Transport*, John Wiley & Sons, New York, 1984.

[12] Kalos, M. H. and Whitlock, P. A., *Monte Carlo Methods, Vol. 1: Basics*, John Wiley and Sons, 1986.

[13] K. Kobayashi, "A Proposal for 3D Radiation Transport Benchmarks for Simple Geometries with Void Region," *OECD Proceedings*, 1997, pp. 403-410.

[14] K. Kobayashi, N. Sugimura and Y. Nagaya, "3D Radiation Transport Benchmarks for Simple Geometries with Void Region", *Proceeding of the Mathematics and Computation, Reactor Physics and Environmental Analysis in Nuclear Applications*, Madrid, Spain, September 27-30, 1999, Vol. 1, p. 657-666.